P H Y S I C A L   R E V I E W   L E T T E R S

Thermal Noise Influences Fluid Flow in Thin Films during Spinodal Dewetting

R. Fetzer,[1,*] M. Rauscher,[2] R. Seemann,[3] K. Jacobs,[1] and K. Mecke[4,†]

[1]*Department of Experimental Physics, Saarland University, 66041 Saarbrücken, Germany*
[2]*Max-Planck-Institut für Metallforschung, Heisenbergstraße 3, 70569 Stuttgart, Germany*
[3]*Max-Planck-Institut für Dynamik und Selbstorganisation, Bunsenstraße 10, 37073 Göttingen, Germany*
[4]*Institut für Theoretische Physik, Universität Erlangen-Nürnberg, Staudtstraße 7, 91058 Erlangen, Germany*

Experiments on dewetting thin polymer films confirm the theoretical prediction that thermal noise can strongly influence characteristic time scales of fluid flow and cause coarsening of typical length scales. Comparing the experiments with deterministic simulations, we show that the Navier-Stokes equation has to be extended by a conserved bulk noise term to accomplish the observed spectrum of capillary waves. Because of thermal fluctuations the spectrum changes from an exponential to a power law decay for large wave vectors. Also the time evolution of the typical wave vector of unstable perturbations exhibits noise-induced coarsening that is absent in deterministic hydrodynamic flow.

With the advent of nanofluidics in the last years it has became evident that thermal noise may play an important role in all hydrodynamic processes occurring at free interfaces on small scales. Although in bulk fluids hydrodynamic Navier-Stokes equations are proven to be valid down to the nanometer scale, in free interface flow stochastic forces induced by molecular motion can significantly alter the behavior even on a micrometer scale. Moseler and Landman, for instance, found that the deterministic lubrication approximation for axial-symmetric free boundary flow is not applicable for the description of nanoscopic cylindrical jets [1]. The lack of thermally triggered fluctuations in the classical hydrodynamic continuum modeling was identified as the most likely source for deviations of the Navier-Stokes equation from molecular dynamics simulations. They derived a stochastic differential equation that includes thermal noise, whose influence on the dynamics increases as the radius of the nanojet becomes smaller, leading finally to the emergence of symmetric double cone neck shapes during the breakup instead of a long thread solution as expected in the absence of noise. In Ref. [2] path integral methods were applied to confirm that thermal noise induces indeed qualitative changes in the breakup of a liquid nanometer jet: Thermal fluctuations speed up the dynamics and make surface tension an irrelevant force for the breakup. Very recently, the importance of thermal noise for drop formation was observed in a colloidal dispersion with an ultralow surface tension [3].

Dewetting of thin films is another technologically important free surface flow problem where a lubrication approximation is used widely. So far, thin film flow has been studied by hydrodynamic Navier-Stokes equations without considering thermal noise, e.g., [4]. With decreasing film thickness, however, it is expected that thermal noise gains significance [5]. In Refs. [5–7], thermal fluctuations have been taken into account and a stochastic

version of the thin film equation was derived based on the lubrication approximation for stochastic hydrodynamic equations [8,9]. The magnitude of the added stochastic forces increases as the thickness of the film decreases. Recent analytical and numerical studies of the stochastic thin film evolution indicate that thermal noise increases characteristic time scales of the dewetting process [6] and changes qualitatively the time evolution of the film thickness $h(\mathbf{r}, t)$ [with $\mathbf{r} = (x, y)$], i.e., its power spectrum $\tilde{C}(q, t)$ [5]. Here, we report that these predictions of noisy hydrodynamics can be confirmed experimentally by *in situ* atomic force microscopy (AFM) of dewetting thin polymer films.

For the experiments, we used polystyrene (PS) of 2.05 kg/mol molecular weight, prepared on silicon wafers with a 191 nm thick silicon oxide layer. By spin casting a toluene solution of PS we prepared films with thicknesses of (3.9 ± 0.5) nm and (4.6 ± 0.5) nm (as measured by ellipsometry at different sites). These films are unstable and dewet spinodally. Above the glass transition temperature, the PS film is liquid and capillary waves can be observed [10]. Below a characteristic wave number their amplitudes grow exponentially in time, eventually leading to holes in the film [11–13]. Dewetting then proceeds by the growth of holes and their coalescence. By tapping mode™ AFM, the entire dewetting process can be monitored *in situ*; cf. Fig. 1.
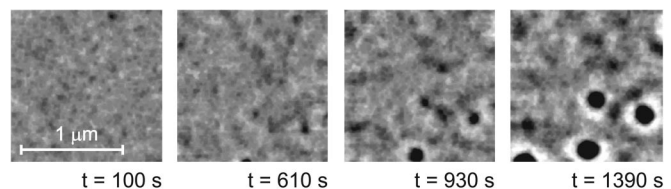

FIG. 1. Dewetting of a 3.9 nm polystyrene film as monitored by *in situ* AFM at 53 °C.

In addition to the experiments, we use deterministic simulation data of the spinodal dewetting process from Ref. [14]. In these simulations, the experimental system parameters film thickness, viscosity, and effective interface potential $\Phi(h)$ were used. We gain quantitative information about the influence of thermal noise to the dewetting process by analyzing the variance $\sigma^2(t) = \overline{h^2} - \overline{h}^2$ of the film height $h(\mathbf{r}, t)$ and the variance $k^2(t) = \overline{(\nabla h)^2}/[2\pi\sigma^2(t)]$ of the local slope of $h(\mathbf{r}, t)$. The quantity $k^2(t)$ gives information about the preferred wave vector within the film surface in the early stage of dewetting before holes are formed; cf. Fig. 1. In this early stage regime, the overbars represent an integration over all positions of the image. During the later stage, however, when holes appear and grow, the linearization of the thin film equation (TFEq) [5], which we use to analyze the data, is in general not valid, but may still be used in between the holes, where the film heights are close to the prepared film thickness h_0. We therefore analyze in the later stage of dewetting the film only at regions where $h(\mathbf{r}, t) \approx h_0$ and ignore the other parts. Note that this spatially selective data analysis is not possible by using correlation function or Fourier space techniques.

A main problem in the data analysis is the finite size of the observation window and the emergence of growing holes in the thin film which limits the film regions where linear dynamics can be studied. The variances σ^2 and k^2 (which are moments of the spectrum) cannot be determined accurately from the Fourier transform of the AFM images. The measured spectrum is convoluted with the Fourier transform of the observation window, which decays as $\sim q^{-2}$ for a sharp cutoff. Thus, the short-wavelength behavior of the spectrum is in our case dominated by the edges of the AFM image and not by the thermal fluctuations. Moreover, the exponentially damped spectrum $\tilde{C} \sim e^{-2t|\omega(q)|}$, characteristic for the deterministic dynamics, is masked by this convolution yielding a spectrum similar to the algebraic noise-induced $\tilde{C}_{\mathrm{CW}}(q) \sim q^{-2}$ [5]. Since the "bare" spectrum $\tilde{C}(q)$ is experimentally not accessible, one has to determine variances σ^2 and k^2 from the real space images. Whereas determining σ^2 is straightforward, calculating k^2 from pixelized images using numerical differentiation is too inaccurate.

Here, we apply an analysis technique based on Minkowski functionals M_ν [14]. We threshold the images at a certain film height h and measure the area $M_0(h)$, boundary length $M_1(h)$, and Euler number $M_2(h)$ as function of h. In the linear regime of spinodal dewetting, the fluctuations in these quantities should follow a Gaussian distribution which was previously tested in Ref. [14]. Then, the mean values of $M_\nu(h)$ depend only on the variances σ^2 and k^2, which can be determined as fit parameters to the functions $M_\nu(h)$. In Fig. 2 we show the resulting temporal evolution of $\sigma^2(t)$ and of $k^2(t)$ in the linear regime. Besides providing accurate estimations of these values, this morphometric analysis allows us to test whether the analyzed
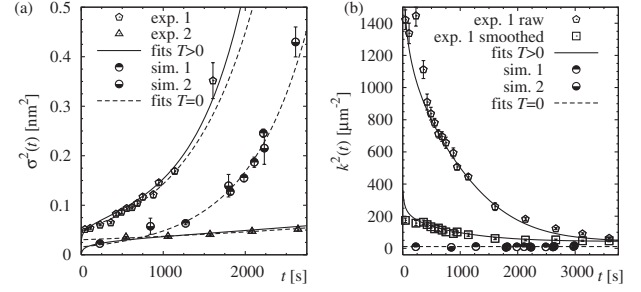

FIG. 2. Analysis of AFM experiments and of deterministic simulations ($T = 0$): (a) The roughness $\sigma^2(t)$ and (b) the variance $k^2(t)$ of the local slope (only experiment 1 and simulations for clarity) as functions of time and fits based on the linearized TFEq. While $\sigma^2(t)$ can be fitted with the deterministic theory by adjusting the initial roughness σ_0^2 and the characteristic time scale t_0, this is not possible for the experimental $k^2(t)$. In the linear regime the deterministic $k^2(t)$ is constant in time.

film region is still in the linear regime. As soon as the nonlinear dynamics sets in, the Gaussian model fails to fit the measured functions $M_\nu(h)$. We compare the data from two experiments at two spatial resolution lengths (experiment 1: pixel size $r_p \approx 6$ nm, temperature $T \approx 53\,°\mathrm{C}$; experiment 2: $r_p \approx 40$ nm, $T \approx 65\,°\mathrm{C}$) with data from deterministic simulations at similar physical conditions and find substantial differences. In the following, we explain these differences by introducing thermal noise to the description of thin film flow.

In both experiments the short chain PS film can be described as an incompressible Newtonian liquid (with a shear viscosity on the order of $\eta \approx 10^4$ N s/m^2) on an infinite, flat solid substrate. Thus, the flow can be modeled by a stochastic Navier-Stokes equation with an additional random stress fluctuation tensor representing the effect of thermal molecular motion [8,9]. We assume no-slip boundary conditions between liquid and substrate and full-slip at the liquid/air interface $z = h(\mathbf{r}, t)$. At the latter, the normal stress is balanced by the surface tension γ and the disjoining pressure $-\Phi'$. For a smooth thin film, where the characteristic film height $h_0 \approx 4$ nm is much smaller than the length scale ≈ 100 nm over which the film thickness varies laterally, a long wavelength expansion yields the following stochastic TFEq [4–6]

$$\frac{\partial h}{\partial t} = \nabla\left(\frac{h^3}{3\eta}\nabla[\Phi'(h) - \gamma\Delta h] + \sqrt{\frac{2k_B T h^3}{3\eta}}\mathbf{N}(t)\right) \quad (1)$$

with a single multiplicative conserved noise vector $\mathbf{N}(\mathbf{r}, t)$ obeying $\langle\mathbf{N}(\mathbf{r}, t)\rangle = 0$ and $\langle N_i(\mathbf{r}, t)N_j(\mathbf{r}', t')\rangle = \delta_{ij}\delta(\mathbf{r} - \mathbf{r}')\delta(t - t')$, where $\langle\cdot\rangle$ denotes the ensemble average over realizations of the noise. The characteristic lateral length scale for a thin film of $h_0 = 4$ nm is given by the spinodal wavelength $2\pi/q_0 = \sqrt{-8\pi^2\gamma/\Phi''(h_0)} = 4h_0^2\sqrt{\pi^3\gamma/A}$, where the Hamaker constant A determines the effective interface potential $\Phi(h) = -\frac{A}{12\pi h^2}$. For the wavelength of the fastest growing mode we find $\frac{2\pi}{q_0} \approx 400$ nm with the

values $A \approx 2 \times 10^{-20}$ N m and $\gamma \approx 3 \times 10^{-2}$ N m determined experimentally for the same system [10]. The experimental parameters lead to dimensionless amplitudes of the noise $\frac{3k_B T}{8\pi^2 h_0^2 \gamma} \approx 4 \times 10^{-4}$ and 2×10^{-4} for experiments 1 and 2, respectively. In the following, we show that even this small current induced by thermal fluctuations can substantially influence the dewetting process.

Comparing the experiments with the numerical solution of Eq. (1) with $T = 0$, we indeed find excellent agreement of the spatial structures [14]. Nevertheless, the time scales do not match. This can be illustrated by comparing the time dependence of $\sigma^2(t)$ and $k^2(t)$ for the AFM data and the deterministic thin film simulations; see Fig. 2. The most significant deviation is observed for $k^2(t)$ which varies in time for the experiments, but stays constant for the deterministic simulations. This mismatch in $k^2(t)$ is most prominent for short times, i.e., for small $\sigma^2(t)$. In the following, we quantitatively analyze the early stages of dewetting in a linear approximation of Eq. (1) to demonstrate the relevance of thermal noise in hydrodynamics on small length scales.

In the beginning of the dewetting process the deviations $\delta h(\mathbf{r}, t) = h(\mathbf{r}, t) - h_0$ from the initial film height h_0 are small as compared to h_0. By expanding Eq. (1) in first order of δh and $\mathbf{N}$ we obtain a linear stochastic equation in Fourier space. Its dispersion relation $\omega(q) = [1 - (q^2/q_0^2 - 1)^2]/t_0$ has its maximum at $q_0^2 = -\Phi''(h_0)/(2\gamma)$ and a characteristic time scale $t_0 = 3\eta/(\gamma h_0^3 q_0^4)$ (about 300 and 1700 s for experiments 1 and 2, respectively). The spectrum reads $\tilde{C}(q, t) = \langle \delta\tilde{h}(\mathbf{q}, t)\delta\tilde{h}^*(\mathbf{q}, t) \rangle = \tilde{C}_0(q)e^{2\omega(q)t} + \frac{k_B T h_0^3}{3\eta}\frac{q^2}{\omega(q)}[e^{2\omega(q)t} - 1]$ with the initial spectrum $\tilde{C}_0(q)$ at $t = 0$. We assume the initial spectrum to be constant $\tilde{C}_0(q) = \frac{2\pi}{q_0^2}\sigma_0^2$ for $q < \sqrt{2}q_0$ and zero otherwise. The spectrum has necessarily a small-scale cutoff $q_m = 2\pi/r_m \gg q_0$ at the scale r_m, which is certainly larger than the fluid molecules. The cutoff for the measured spectrum is set by the experimental resolution, e.g., by the pixel size r_p or a smoothing length if the data are postprocessed. Because of a rapid buildup of noise-induced short-wavelength roughness on a short time scale $t_m = (q_0/q_m)^4 t_0$, the short-wavelength part of the initial spectrum $\tilde{C}_0(q > q_0)$ is irrelevant for the film evolution on the characteristic time scale $t_0 \gg t_m$.

In the case of a spinodally unstable film with $\Phi''(h_0) < 0$ the dispersion relation $\omega(q)$ is negative for $q > \sqrt{2}q_0$. This leads to two important differences between deterministic and stochastic dewetting. First, and largely independent of the initial roughness, for $t \to \infty$ and $q > \sqrt{2}q_0$ one finds an exponentially decaying power spectrum $\tilde{C}(q, t) \to \tilde{C}_0(q)e^{-2|\omega(q)|t}$ in the deterministic dynamics ($T = 0$) but we recover the algebraic capillary wave spectrum $\tilde{C}(q, t) \to \frac{k_B T h_0^3}{3\eta}\frac{q^2}{|\omega(q)|} \sim \frac{k_B T}{\gamma q^2} = \tilde{C}_{CW}(q)$ for any finite temperature T. And second, for sufficiently smooth initial

spectra which decay rapidly for $q > \sqrt{2}q_0$, the maximum of the deterministic spectrum stays at q_0 for all times, while the maximum of the stochastic spectrum approaches q_0 from above as $t \to \infty$; see Ref. [5] for details. This noise generated coarsening process can last until nonlinearities become important, effectively masking the most typical feature of the linear deterministic regime, namely, that the maximum of the power spectrum stays at the fixed wave number q_0.

In order to further illustrate the spatiotemporal features of the dynamics we calculate the time evolution of the roughness of the film $\sigma^2(t) = \int \frac{d^2 q}{(2\pi)^2}\tilde{C}(q, t)$ shown in Fig. 2(a) for the experiments discussed above and the corresponding deterministic simulation. Both the experimental and the deterministic data can be fitted with the deterministic $\sigma^2_{T=0}(t)$ with parameters t_0 and σ_0 in reasonable agreement with the experimental parameters. The initial roughness σ_0^2 is experimentally not accessible. Thus, the time evolution of the roughness $\sigma^2(t)$ gives no clear indication for the importance of thermal fluctuations for the dewetting process.

Yet, the variance of the local slope $2\pi\sigma^2(t)k^2(t) = \langle [\nabla\delta h(\mathbf{r}, t)]^2 \rangle = \int \frac{dq q^3}{2\pi}\tilde{C}(q, t)$ is sensitive to thermal noise. We find a strong dependence on the noise term for times $t \sim t_0$, whereas the late stage $k^2(t \to \infty) = k_0^2$ is given by the maximum of the dispersion relation $k_0^2 = q_0^2/(2\pi)$ alone. The reason why the noise term becomes irrelevant for large t is the strong increase of $\sigma^2(t)$ with time due to the deterministic growth of unstable modes. Note that for a purely deterministic dynamics the variance $k^2_{T=0}(t) = k_0^2$ changes in time only at short time scales t_m and remains constant in time if one chooses $q_m = \sqrt{2}q_0$. In particular, the position $q \approx k(t)$ of the maximum in the structure function $\tilde{C}(q, t)$ does not change during a deterministic dewetting process. In contrast, thermal noise induces a time dependence of $k^2(t)$. The experimental data cannot be fitted with the deterministic theory, because $k^2(t)$ is clearly not constant in time. A simultaneous fit to the experimental data with $\sigma_0^2 = 0$ yields $k_B T/(4\pi\gamma)$ and the cutoff wave vector q_m^2/q_0^2 as given in Table I. From the experimental parameters we would expect $k_B T/(4\pi\gamma) \approx 0.012$ nm^2 for both experiments, which is reasonably close to the fitted values. The values for q_m correspond to cutoff lengths r_m which are larger than the nominal pixel size. The reason is probably that the experimental cutoff is smooth rather than sharp. However, the ratios of the r_m for the different experiments matches quite well the ratios

TABLE I. Experimental fit parameters for Figs. 2 and 3.

Dataset	$\frac{k_B T}{4\pi\gamma}$ [nm^2]	$\frac{q_m^2}{q_0^2}$	k_0^2 [μm^{-2}]	χ	r_m [nm]
1 smooth	0.01	12	48	5.6×10^{-6}	116
1 raw	0.01	170	40	7×10^{-5}	33
2 raw	0.008	28	9	2.5×10^{-6}	174

of the corresponding pixel sizes. In contrast to σ_0^2, smoothing changes k^2 drastically. Deterministic simulation data are hardly affected by smoothing. Smoothing obviously removes fluctuations on small scales, which are exponentially fast damped by the deterministic dynamics but are permanently (re)generated by thermal noise in the experiments. A quantitative analysis of the experiments at different lateral resolution clearly confirms thermal noise as the most likely source for the observed k^2 dependence. The dependence of k^2 on the upper cutoff q_m is a crucial test of the theoretical prediction as presented below in Eq. (2).

As the small-scale cutoff q_m is much larger than q_0 there is a time regime $t > t_m \approx 10^{-2} t_0$ up to $t \approx t_0$ where $k^2(t)$ is approximately given by

$$k^2(t) \approx k_0^2 + \frac{\chi}{\sigma^2(t)}, \quad \text{with} \quad \chi = \frac{k_B T q_m^2}{8\pi^2 \gamma}, \qquad (2)$$

independent of the initial conditions [5]. Since $\sigma^2(t)$ is monotonically increasing with time, the characteristic wavelength $\sqrt{2\pi/k^2(t)}$ increases. Thus, thermal noise generates coarsening even in the linear regime for which the deterministic linear dynamics predicts a fixed characteristic wave vector. Figure 3 shows k^2 as a function of σ^2 fitted by Eq. (2) as well as by the full linear stochastic theory. Both fits give consistent values for k_0^2 and χ which are given in Table I. These values are also consistent with the values determined by the system parameters given above.
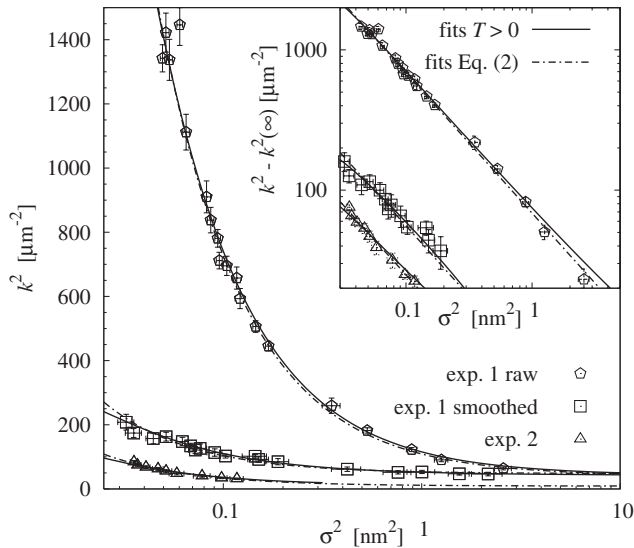
From the fit values k_0^2 and the theoretical relation $q_0^2 = -\Phi''(h_0)/(2\gamma)$ we get in experiment 1 for the film thickness 3.6 and 3.8 nm from the smoothed and raw data, respectively, and for experiment 2 $h_0 = 5.5$ nm. These values are in good agreement with our experimental data. Accordingly, one finds from the fit values for χ the cutoff lengths r_m given in Table I—in good agreement with the ratios of pixel sizes and smoothing length, respectively. It is remarkable that one can determine reliable values for film thicknesses and lateral resolution by measuring the effect of thermal noise on fluid flow. This is a strong indication that the coarsening visible in $k^2(t)$ during the linear regime is indeed due to thermal fluctuations which can be described by the stochastic TFEq (1). Numerical solutions of Eq. (1) would provide an excellent further test.

In conclusion, the interplay of substrate potentials and thermal noise can strongly influence characteristic time scales of fluid flow and leads to a coarsening of typical lengths on a μm scale. The results will have an impact on the future development of nanofluidics, enabling reliable predictions of fluid flow in confined geometries such as in liquid coatings or in lab-on-chip devices.

FIG. 3.   Slope variance k^2 from the experiments plotted versus the roughness σ^2. The solid lines are fits based on the linearized stochastic TFEq, whereas the dash-dotted lines are asymptotic fits according to Eq. (2). The influence of noise is reduced for smoothed as well as for less resolved data (experiment 2). The inset shows the same data in a double logarithmic plot highlighting the validity of the asymptotic equation (2).

*Present address: Ian Wark Research Institute, University of South Australia, Mawson Lakes, SA 5095, Australia.
†mecke@physik.uni-erlangen.de

[1] M. Moseler and Uzi Landman, Science **289**, 1165 (2000).
[2] J. Eggers, Phys. Rev. Lett. **89**, 084502 (2002).
[3] Y. Hennequin *et al.*, Phys. Rev. Lett. **97**, 244502 (2006).
[4] A. Oron, S. H. Davis, and S. G. Bankoff, Rev. Mod. Phys. **69**, 931 (1997).
[5] K. Mecke and M. Rauscher, J. Phys. Condens. Matter **17**, S3515 (2005).
[6] G. Grün, K. Mecke, and M. Rauscher, J. Stat. Phys. **122**, 1261 (2006).
[7] B. Davidovitch, E. Moro, and H. A. Stone, Phys. Rev. Lett. **95**, 244505 (2005).
[8] L. D. Landau and E. M. Lifšic, *Statistische Physik* (Akademie Verlag, Berlin, 1991), 5th ed.
[9] R. F. Fox and G. E. Uhlenbeck, Phys. Fluids **13**, 1893 (1970).
[10] R. Seemann, S. Herminghaus, and K. Jacobs, Phys. Rev. Lett. **86**, 5534 (2001); J. Phys. Condens. Matter **13**, 4925 (2001).
[11] A. Vrij, Discuss. Faraday Soc. **42**, 23 (1966).
[12] E. Ruckenstein and R. K. Jain, J. Chem. Soc., Faraday Trans. 2 **70**, 132 (1974).
[13] S. Herminghaus *et al.*, Science **282**, 916 (1998).
[14] J. Becker, G. Grün, R. Seemann, H. Mantz, K. Jacobs, K. Mecke, and R. Blossey, Nat. Mater. **2**, 59 (2003).